remote sensing

MDPI

Article

A Spectral Library Study of Mixtures of Common Lunar Minerals and Glass

Xiaoyi Hu [1,2], Te Jiang [1], Pei Ma [1], Hao Zhang [1,3,*], Paul Lucey [4] and Menghua Zhu [5]

[1] Planetary Science Institute, School of Earth Sciences, China University of Geosciences, Wuhan 430074, China
[2] Institute of Seismology, China Earthquake Administration, Wuhan 430071, China
[3] CAS Center for Excellence in Comparative Planetology, Hefei 230026, China
[4] Hawaii Institute of Geophysics and Planetology, University of Hawaii, Honolulu, HI 96822, USA
[5] State Key Laboratory of Lunar and Planetary Sciences, Macau University of Science and Technology, Macau 999078, China
* Correspondence: zhanghao@cug.edu.cn

Abstract: Reflectance spectroscopy is a powerful tool to remotely identify the mineral and chemical compositions of the lunar regolith. The lunar soils contain silicate minerals with prominent absorption features and glasses with much less distinctive spectral features. The accuracy of mineral abundance retrieval may be affected by the presence of glasses. In this work, we construct a spectral library of mixtures of major lunar-type minerals and synthetic glasses with varying relative abundances and test their performance on mineral abundance retrievals. By matching the library spectra with the spectra of mineral mixtures with known abundances, we found that the accuracy of mineral abundance retrieval can be improved by including glass as an endmember. Although our method cannot identify the abundance of glasses quantitatively, the presence or absence of glasses in the mixtures can be decisively determined.

Keywords: lunar glass; mineral abundance retrievals; radiative transfer models

Citation: Hu, X.; Jiang, T.; Ma, P.; Zhang, H.; Lucey, P.; Zhu, M. A Spectral Library Study of Mixtures of Common Lunar Minerals and Glass. *Remote Sens.* **2023**, *15*, 2195. https://doi.org/10.3390/rs15082195

Academic Editor: Giancarlo Bellucci

Received: 21 February 2023
Revised: 9 April 2023
Accepted: 18 April 2023
Published: 21 April 2023

1. Introduction

The mineral composition and abundance of lunar surface materials contain a rich record of the thermal and chemical evolutions of the Moon [1,2]. Reflectance spectroscopy is one of the most useful tools to study the mineralogy of the lunar surface [3,4], as many lunar minerals have diagnostic absorption features in visible and near-infrared (VNIR) spectral regions from 0.5 to 2.5 μm. It is well known that olivine (OLV), clinopyroxene (CPX), orthopyroxene (OPX), plagioclase (PLG), ilmenite (ILM), and glasses are the major endmembers of the lunar surface minerals. As shown in Figure 1, OLV has a broad absorption near 1000 nm which can be resolved into three overlapping absorptions centered around 850 nm, 1050 nm, and 1250 nm [5,6]; pyroxenes (PYX, including CPX and OPX) have two diagnostic absorptions near 1000 nm and 2000 nm [7]. PLG has a weak absorption centered at 1250 nm, and ILM is an opaque oxide that is nearly spectrally featureless [8].

In addition, the lunar regolith contains a fairly large amount of glassy materials, including impact and volcanic glasses produced by impact melting and explosive volcanism, respectively [9]. Impact glass is produced during meteoroid or micrometeoroid bombardment, which melts and welds rock, mineral, and glass fragments to produce agglutinate, which may account for more than 50 wt.% of the lunar regolith [10–12]. The agglutinates include melt glass, devitrified material, amorphous rinds, and dark (translucent or opaque) amorphous material [13]. These multi-component, highly irregular particles are typically very dark and often contain lithic fragments embedded in melt glass. Lunar volcanic glasses are believed to come from a deep interior source and are recognized as a good geochemical and petrologic probe into the lunar mantle [14,15]. The lunar green/orange

glasses and black beads were found at specific Apollo landing sites on the Moon and represent quenched volcanic glasses that give insight into lunar magma compositions and deep volatile contents [16,17]. Green and orange glasses in the form of spheroidal beads, broken beads, and irregular fragments have been found at Apollo 15 and 17 landing sites [18]. Moreover, these two glass samples are found to be rather homogeneous in composition and are often used as glass endmembers in lunar material studies [14,19].

Even for silicates with prominent absorption features, the quantitative endmember's abundance retrieval from the reflectance spectra of their mixtures is not straightforward, and thus radiative transfer models [20] need to be used [21,22]. The presence of glassy materials with varied chemical compositions and complex structures further complicates mineral abundance retrievals [23], as lunar volcanic glasses have broad and shallow absorption features near 1000 nm and 2000 nm (Figure 1) that overlap with silicate absorptions [24].

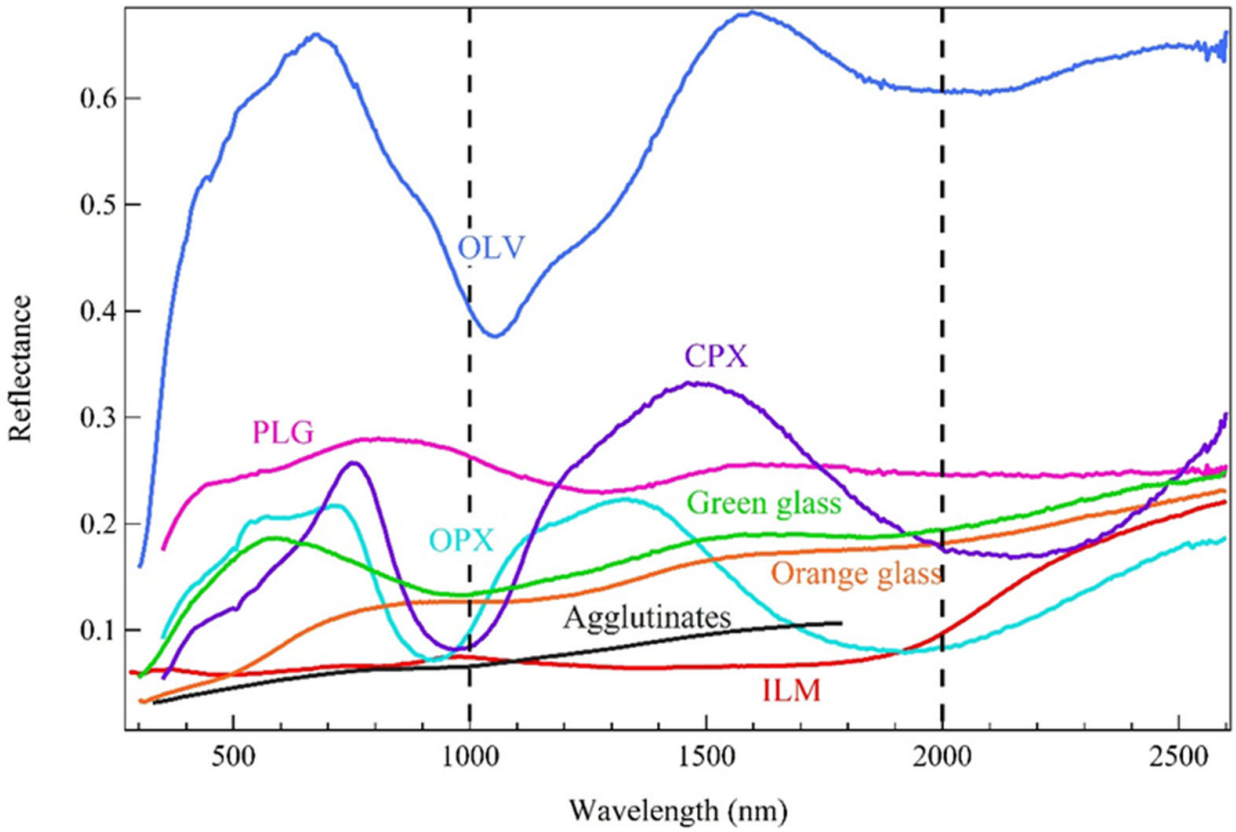

Figure 1. Laboratory reflectance spectra measured at incident zenith angle i = 30°, emission angle e = 0°, and phase angle g = 30° of representative lunar minerals and glasses. Dashed lines at 1000 and 2000 nm indicate the major absorption features of the silicates. The Reflectance Experiment Laboratory IDs are LR-CMP-014 for OLV, LS-CMP-004 for PLG, LS-CMP-009 for CPX, LS-CMP-012 for OPX, LR-CMP-052 for green glass, LR-CMP051 for orange glass, and LR-CMP-182 for ILM. The agglutinate is the Apollo 15,041 agglutinates spectrum from [25].

By far, most mineral abundance retrieval studies concentrate on mixtures of silicate minerals, and the glass abundance information is mostly unavailable [26,27]. As modern spaceborne and in situ sensors have measured lunar surface reflectance spectra with higher spatial and spectral resolutions, there are increasing need and possibility to retrieve glass abundance. In this work, we constructed a spectral library that includes both silicates and volcanic glasses as endmembers. We then used the library to derive the mineral abundances from measurement spectra of lunar soils from the Lunar Samples Characterization Consortium (LSCC) [8,28] and mineral mixtures from the Reflectance Experiment Laboratory (RELAB) [29]. Finally, the spectral library is applied to the Chang'E-3 (CE-3) in situ

reflectance spectra [26,30,31] to infer the presence of glass and improve the accuracy of mineral abundance retrievals. The scattering geometry for both the LSCC and RELAB measurements are incident zenith angle $i = 30°$, emission angle $e = 0°$, and phase angle $g = 30°$.

2. Method and Data

2.1. Model Descriptions

We use the Hapke model [32] to describe the spectral reflectance in reflectance factor (REFF) at each wavelength as

$$r(i,e,g) = K\frac{\omega}{4}\frac{1}{cos\ i + cos\ e} \times \left\{p(g)[1+B(g)] + H\left(\frac{cos\ i}{K}\right)H\left(\frac{cos\ e}{K}\right) - 1\right\}, \quad (1)$$

where ω is the single scattering albedo (SSA), i, e, and g, the incident zenith, viewing zenith, and the phase angle that is fixed at 30°, 0°, and 30°, respectively. K is the porosity factor that can be calculated from the filling factor ϕ as [20]

$$K = \frac{-ln\left(1 - 1.209\phi^{\frac{2}{3}}\right)}{1.209\phi^{\frac{2}{3}}}. \quad (2)$$

$B(g)$ describes the shadow hiding opposition effect (SHOE) with an angular half width at half maximum h_s as

$$B(g) = \left(1 + \frac{tan(g/2)}{h_s}\right)^{-1}. \quad (3)$$

For equant particles larger than the radiation wavelength and with a narrow particle size distribution, h_s can be estimated by

$$h_s = \frac{3\sqrt{3}}{8}\frac{K\phi}{ln(1000)}. \quad (4)$$

with a typical ϕ value of 0.41, Equation (4) gives a h_s value of 0.0636. The single particle scattering phase function $P(g)$ is approximated by

$$P(g) = 1 + bcos(g) + c\left(1.5cos^2(g) - 0.5\right), \quad (5)$$

where the empirical values of $b = -0.4$ and $c = 0.25$ derived by Mustard and Pieters [33] are used. The H function in Equation (1) is approximated by

$$H(x) = \left[1 + \omega x\left(r_0 + \frac{1 - 2r_0x}{2}ln\frac{1+x}{x}\right)\right]^{-1}, \quad (6)$$

where

$$r_0 = \frac{2}{1 + \sqrt{1-\omega}} - 1, \quad (7)$$

with x is either *cosi/K* or *cose/K*. The reflectance and the SSA can be easily converted to each other using the Hapke model (Equations (1)–(7)).

With the real and imaginary refractive index n and k of a grain, the SSA can be approximated by the equivalent slab model [26] as

$$\omega = S_e + (1 - S_e)(1 - S_i)\frac{\Theta}{1 - S_i\Theta}, \quad (8)$$

where

$$S_e = \frac{(n-1)^2}{(n+1)^2} + 0.05, \quad (9)$$

$$S_i = 1.014 - \frac{4}{n(n+1)^2}. \tag{10}$$

The S_e and S_i are the integral of external and internal Fresnel reflection coefficients of all the grains, and the Θ is the particle internal transmission factor, and when the absorption coefficient $\alpha << 1$, it can be approximated as

$$\Theta \approx e^{-\alpha\langle D\rangle}. \tag{11}$$

where

$$\alpha = \frac{4\pi k}{\lambda}, \tag{12}$$

$\langle D\rangle$ is the average grain size approximated by the thickness of the equivalent slab, and it can be calculated with the average grain size D,

$$\langle D\rangle = \frac{3}{2}\left[n^2 - \frac{1}{n}\left(n^2-1\right)^{\frac{3}{2}}\right]D. \tag{13}$$

Using the intimate mixture model (e.g., [21]), the SSA of a mixture can be calculated in terms of that of the endmembers:

$$\omega_{mix} = \frac{\sum_i \frac{M_i\omega_i}{\rho_i D_i}}{\sum_i \frac{M_i}{\rho_i D_i}}, \tag{14}$$

where ω_i, M_i, ρ_i, and D_i are the SSA, the bulk density, the solid density, and the grain size of the i^{th} endmember, respectively.

2.2. Synthetic Glass Spectra

The VNIR spectral features of lunar volcanic glasses are mostly controlled by chemistry contents, especially iron (Fe) and titanium (Ti) [19]. Based on the various chemical compositions of the Apollo samples, Cannon et al. [19] synthesized several analog materials, including the green, yellow, orange, crust, mare, and red pyroclastic glasses, which have similar spectral features above 1000 nm, but different reflectance values. Figure 2a shows the VNIR spectra of the synthetic green and orange glasses produced by Cannon et al. [19] together with several Apollo agglutinates. The chemical compositions of the synthetic lunar green and orange glasses are shown in Table 1. Similar to the typical lunar volcanic glasses shown in Figure 1, the synthetic green and orange glasses have absorptions around 1000 nm and 2000 nm. The reflectance peaks near 550 nm and 700 nm give rise to their characteristic green and orange colors, respectively. In contrast, the agglutinates containing nanophase irons show reddened spectra with very weak absorptions around 1000 nm. Since these synthetic orange and green glasses are well-sorted in size distributions and have spectral features similar to lunar volcanic glasses, they are selected as the glass endmembers in this study.

Table 1. The chemical compositions of the synthetic lunar green and orange glasses (from [19]).

Compositions	SiO_2	TiO_2	Al_2O_3	Cr_2O_3	FeO	MnO	MgO	CaO	Na_2O	K_2O
Synthetic green glass (wt.%)	25.58	0.55	7.89	0.51	19.49	0.28	17.1	8.43	0.19	0.01
Synthetic orange glass (wt.%)	38.39	9.98	6.01	0.66	22.86	0.31	13.87	7.44	0.42	0.06

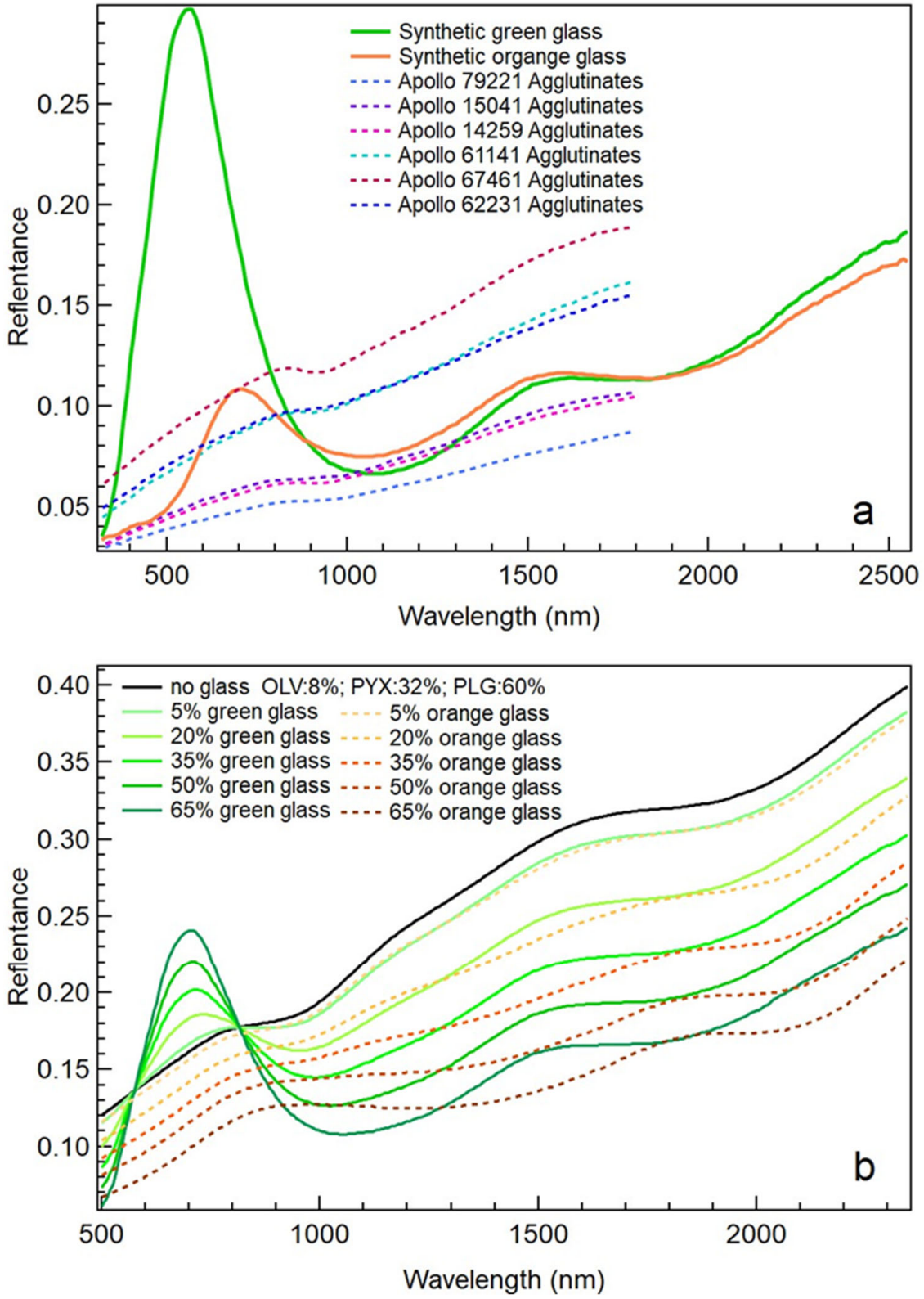

Figure 2. (**a**) The synthetic lunar green and orange glass from [19] and the Apollo sample agglutinates spectra from [25]; (**b**) VNIR spectra from our spectral library. We added a series content of glass to the mineral mixture (OLV:8 wt.%, PYX: 32 wt.%, PLG: 60 wt.%) to highlight the spectral differences between different content of synthetic lunar glasses in this study.

To understand the effects of glass abundance on spectral features, we added synthetic green/orange glass as endmembers to the spectral look-up table (LUT) produced by [34]. Specifically, we used the Hapke model (Equations (1)–(7)) to get the SSA of the mineral mixture and glass and then calculated the mixture's SSA using Equation (14). From the mixture's SSA, we calculated the spectra of the mixture with different glass abundance, shown in Figure 2b. The absorptions at 1000 nm and 2000 nm become broader with the addition of green and orange glasses. For mixtures with green glass, the spectral slope decreases with the increase of glass abundance, and the ~650 nm peak is distinguishable as long as the glass abundance is higher than 20 wt.%. For mixtures with orange glass, the major effect is darkening, and the spectral slope only changes slightly as glass abundance increases. Overall, the spectral characteristics of the mixture change with the addition of glass. It may lead to larger errors in the inversion results if not considering glass.

Cannon et al. [19] mixed basalt with 0–70 wt.% synthetic glass and found that, although the glass abundance retrieved by their unmixing model increases with the increase of true glass abundance, the retrieved glass abundance was underestimated. For example, when 60 wt.% basalt and 40 wt.% synthetic glass were physically mixed, the glass abundance retrieved by the model is only ~20 wt.%. The most likely reason is that the two relatively weak glass absorptions around 1000 nm and 2000 nm are masked by OLV's stronger absorptions in close proximity, as OLV containing a sufficient amount of chromium may have the ~2000 nm absorption, in addition to its intrinsic broad 1000 nm absorption. This example demonstrates that the glass abundance may be retrieved qualitatively but not quantitatively for binary mixtures.

2.3. Spectral Library Construction

The procedure for constructing the spectral mixing library is outlined in Figure 3. We first start with the LUT spectra of OLV, OPX, CPX, and PLG [34,35] and convert their mixture reflectance to SSA using the Hapke model. Then, we calculate the SSA of glass from the spectra of synthesis green/orange glass in the same way (Equations (1)–(7)). Finally, the intimate mixture formula (Equation (14)) and the Hapke model are used to calculate the spectral library of mixtures (MSL) of minerals and glass.

The effective grain size of the minerals in the mixture is fixed at 17 μm, which is a representative value of lunar soil based on the LSCC research [1,13]. Due to laboratory preparation procedures, the synthetic glass grains are smaller than 53 μm. Compared with other glass samples, the particle size distribution of Cannon's synthetic samples is smaller [19] and is closer to the particle size of the lunar regolith. The Mg number is fixed at 65 [34] because the LSCC data has Mg numbers between 50–70. To simulate the reddening and darkening effects caused by space weathering, nanophase irons with weight percentages from 0.0005 wt.% to 0.007 wt.% were added to all library spectra [34]. It should be noted that the synthetic green/orange glass in the MSL differs from the matured lunar glass in that the latter contains a large amount of glass-welded aggregates (~30–50% modal abundance of the LSCC soil). The agglutinate glasses also originated from volcanic and impact processes. Because of the nanophase iron inside the agglutinates [25,36], the absorption of agglutinate has been largely smoothed out, as shown in Figure 2a, and the modification effect of the agglutinate on the spectrum of the lunar regolith is lower than that of volcanic glass. The spectral reddening and darkening due to space weathering is also considered by adding nanophase iron with varying content from 0.0005 wt.% to 0.007 wt.% to the mineral mixture when constructing the MSL (Figure 3). Thus, in this work, we only discuss the simple case of adding volcanic glass as the glass endmember.

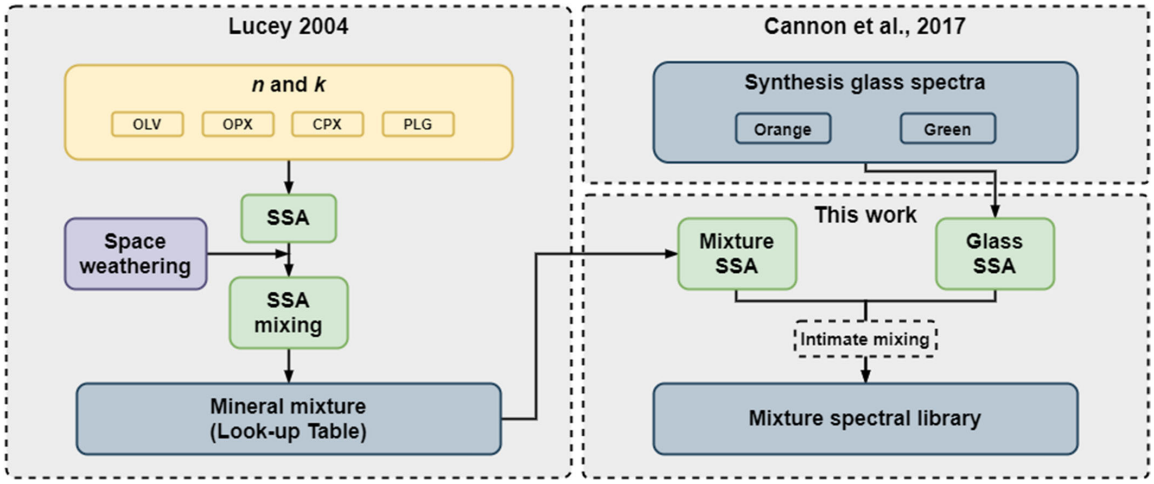

Figure 3. The modeling procedure of constructing the spectral mixing library. We added one of the synthetic glasses, the orange glass or the green glass, to the library [19,34].

Glass varied from 0 to 80 wt.%, and minerals OLV, OPX, CPX, and PLG varied from 0 to 100 wt.%, all in steps of Figure 3, with a total of 100 wt.% of the five endmembers. The resultant library consists of about 700,000 spectra in total.

2.4. Spectral Matching Algorithms

To find the best match between the MSL and target spectra, we tried four selection criteria: the absolute difference (ABS), the normalized absolute difference (NABS), the centered pattern root mean square (CPRMS) [10], and the spectral angle mapper (SAM) as follows:

$$ABS = \sum_{n=1}^{N} |f_n - r_n|, \tag{15}$$

$$NABS = \sum_{n=1}^{N} \left| \frac{f_n}{\overline{f}} - \frac{r_n}{\overline{r}} \right|, \tag{16}$$

$$CPRMS = \sqrt{\frac{1}{N} \sum_{n=1}^{N} \left[\left(f_n - \overline{f} \right) - \left(r_n - \overline{r} \right) \right]^2}, \tag{17}$$

$$SAM = \frac{\sum_{n=1}^{N} f_n r_n}{\sqrt{\sum_{n=1}^{N} f_n^2} \sqrt{\sum_{n=1}^{N} r_n^2}}, \tag{18}$$

where f_n, r_n, f, and r are the *nth* measurement data point, the *nth* MSL spectral data point, the average of measurement, and the average of MSL of N discrete data points, respectively.

3. Results

In order to test the accuracy of the spectral library of mixtures (MSL) constructed, we chose two kinds of data: (1) the Apollo lunar soil spectra from the Lunar Samples Characterization Consortium (LSCC) and (2) the Reflectance Experiment Laboratory (RELAB) spectra of mineral mixtures. The Apollo soil samples characterized by the LSCC represent the most realistic lunar soil conditions, with true abundances measured in the laboratory, while the RELAB samples cover a range of glass-free mineral mixtures and thus can be used to check if the MSL may return spurious glass abundance.

3.1. Test the Accuracy of the MSL by the LSCC Lunar Soil Samples

The LSCC published 19 Apollo soil spectra and their mineral abundances [37,38] (https://sites.brown.edu/relab/lscc/ (accessed on 17 April 2023)). Each soil sample was

wet-sieved into four different grain size distributions: 0–10 μm, 10–20 μm, 20–45 μm, and 0–45 μm [38]. The 10–20 μm sample spectra are selected in this research as this size is closest to the mineral size (17 μm) used in our spectral library [1,34]. We used all 19 samples as test samples and added the symbol X before the sample number to indicate that these samples are 10–20 μm in diameter.

To understand the effect of using glass as an endmember on retrieval accuracy, we used both the MSL with orange glass and the LUT without glass to retrieve the mineral abundances from the LSCC spectra, and the results are shown in Figure 4. From these plots, it can be seen that the ABS criteria favor more on reflectance value while the NABS and SAM favor more on spectral shape. By averaging the results derived using these four metrics, all major spectral features, including the reflectance value, the absorption peak position, and the absorption depth, have been taken into account, and thus the retrieved mineral abundance should be more accurate. Therefore, we used the average of the results from the four evaluation criteria.

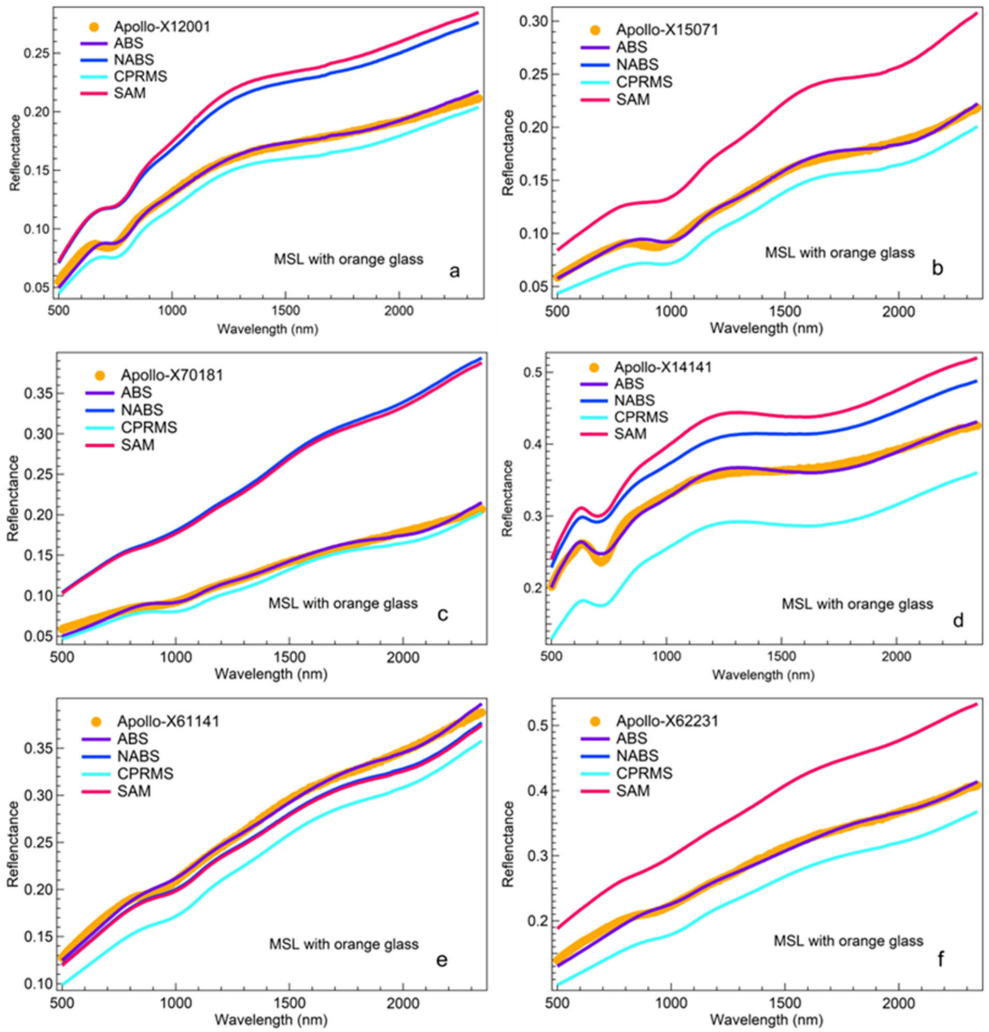

Figure 4. Comparisons of the LSCC measurement spectra with the corresponding best-matched MSL spectra with orange glass were obtained using four different fitting metrics for (**a**) X12001, (**b**) X15071, (**c**) X14141, (**d**) X70181, (**e**) X61141, and (**f**) X62231.

Table 2 lists the relative abundances (wt.%) of three minerals, where PYX is the total of OPX and CPX. Obviously, the relative abundances of minerals retrieved from the MSL with glass are closer to the LSCC measurement value. Figure 5 shows the difference in abundance of the three minerals from the MSL inversion results with and without glass

and the LSCC measurement value. The circles and squares indicate the difference between the LSCC measurement and the MSL retrieval results with and without taking into account glass. The fact that most circles are below the squares indicates that adding glass as the endmember improves retrieval accuracy.

Table 2. Relative abundance (wt.%) of the three minerals (OLV + PYX + PLG = 100 wt.%) retrieved from the MSL with and without considering glass and the LSCC measurement results.

Soil ID	Measurement (wt.%)			MSL (without Glass) (wt.%)			MSL (with Green Glass) (wt.%)			MSL (with Orange Glass) (wt.%)		
	OLV	PYX	PLG	OLV	PYX	PLG	OLV	PYX	PLG	OLV	PYX	PLG
X12001-56	11.7	49.7	38.6	17.9	52.4	29.7	13.5	57.3	29.5	15.18	55.8	29.0
X12030-14	9.5	54.7	35.8	14.4	58.9	26.7	2.4	63.9	33.8	15.6	57.1	27.3
X15041-94	6.9	47.7	45.5	19.1	45.3	35.7	8.1	56.4	34.3	15.9	56.1	28.0
X15071-52	7.2	42.9	49.9	18.5	53.8	27.7	6.5	59.0	34.5	18.3	58.0	23.8
X70181-47	12.4	27.8	59.8	21.2	32.8	46.0	13.1	23.4	63.5	16.8	37.8	45.5
X71061-14	14.0	38.8	47.2	23.5	16.2	60.3	11.8	22.7	65.5	22.6	25.1	52.3
X71501-35	9.2	37.1	53.7	19.4	28.6	51.0	8.5	48.3	43.3	9.6	50.7	39.8
X79221-81	11.7	33.3	55.0	28.3	28.0	43.7	24.6	35.4	40.0	19.0	38.4	42.5
X10084-78	3.6	40.1	56.3	24.8	22.9	52.3	17.0	37.3	45.8	8.6	52.1	49.2
X14141-5.7	4.0	26.9	69.1	10.5	33.1	56.3	9.2	32.1	58.8	10.4	29.2	60.5
X14163-57	6.1	40.4	53.5	6.8	36.5	47.3	1.7	36.8	61.5	9.7	38.3	52.0
X14259-85	5.4	35.1	59.5	4.4	25.3	70.3	5.7	28.3	66.0	7.7	25.1	63.3
X14260-72	5.1	40.7	54.2	6.6	26.4	67.0	7.3	29.0	63.8	4.8	28.2	63.8
X61141-56	3.5	7.3	89.2	3.8	13.2	83.0	1.4	19.7	79.0	5.3	21.0	67.0
X61221-9.2	3.0	8.0	89.1	1.2	35.5	63.3	0.4	27.6	72.0	3.6	23.2	73.8
X62231-91	3.9	10.0	86.1	4.8	22.3	73.7	2.8	14.3	83.0	3.4	11.8	73.3
X64801-82	2.6	7.3	90.1	1.3	16.3	82.3	1.0	14.8	84.3	4.0	9.8	85.8
X67461-25	2.3	6.2	91.6	3.9	10.3	86.3	0.8	12.5	84.5	4.1	15.3	80.5
X67481-31	4.1	7.9	87.9	3.1	6.6	90.3	3.8	8.4	87.8	3.8	8.4	87.8

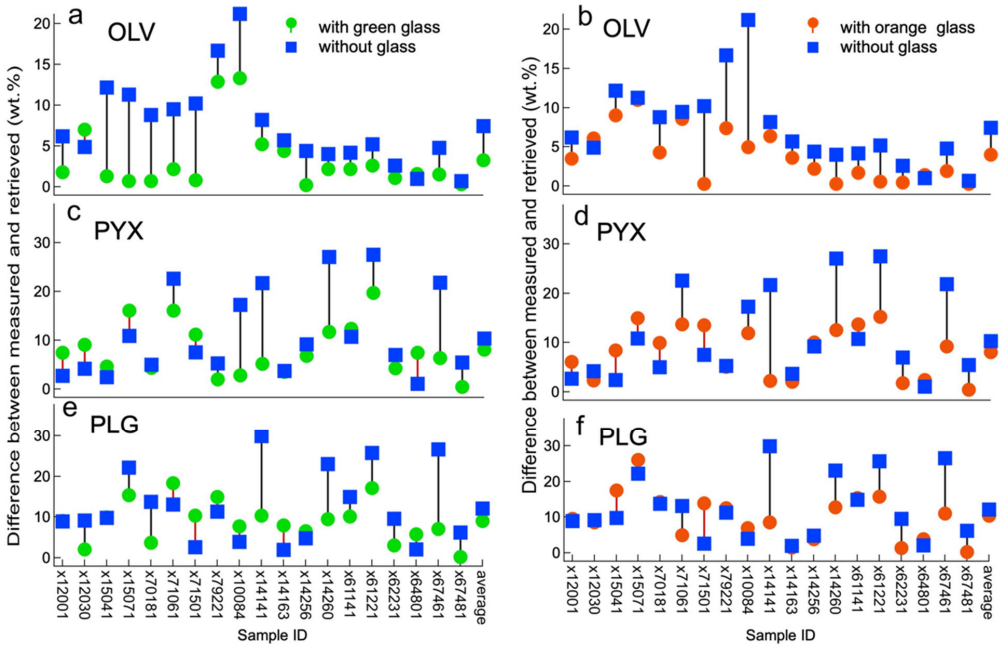

Figure 5. The absolute difference in relative abundance between the MSL retrieval of this work and the LSCC measurement (Difference = |LSCC measurement–MSL retrieval|) for OLV (**a**,**b**), PYX (**c**,**d**), and PLG (**e**,**f**). The blue squares indicate the weight% difference between the measurement and the retrieval with no glass considered. The green and orange circles indicate the weight% difference in retrieved and measured mineral abundances with green and orange glasses, respectively. Vertical black and red lines indicate that the retrieval results with glass considered are closer and further from the actual measurement results, respectively.

Due to the complexity of multivariate mixing, we only added either the orange or green glass as the endmember in the MSL. Although the two types of glasses have some spectral differences, adding either one to the MSL can improve the accuracy of mineral abundance retrievals.

Table 3 shows the glass abundances in lunar soils from the LSCC measurements and the MSL retrieval results. No correlations between the agglutinate abundance and the retrieved glass abundance were found (Table 3), as the agglutinates often contain lithic fragments embedded in melt glass and other absorbing amorphous material. However, for mare soil samples that contain pure volcanic glass, as shown by the LSCC measurements, the MSL retrievals returned higher glass abundance (~7.1 wt.% green glass or ~10.8 wt.% orange glass) than the highland soil samples (~3.1 wt.% green glass or ~4.9 wt.% orange glass). As discussed in Section 2, the retrieved glass abundance may be underestimated. However, a positive value for glass abundance can be retrieved for all the samples. This test shows that, by adding glass as an endmember, not only can glass abundances be retrieved qualitatively, but the accuracy of mineral abundances can also be improved.

The criteria Equations (15)–(18) would return lower values for better-matched datasets. We found the values of ABS, NABS, and CPRMS for the best-matched spectra obtained from MSL with green glass are smaller than that of the results obtained using the MSL with orange glass, which indicates that the green glass is a reasonable endmember for the 19 LSCC samples in mineral abundance retrievals.

3.2. Test the Accuracy of the MSL by the RELAB Samples

To test if the spectral library may return false glass abundance, we used the RELAB spectra of glass-free samples to perform the retrieval. We selected four mixtures of pure lunar-type minerals, including OLV, OPX, CPX, PLG, and ILM, from RELAB, and the sample ID and mineral abundances are summarized in Table 4. We did not consider ILM as an endmember in constructing the MSL because ILM lacks prominent spectral features. All samples are glass-free and have a particle size distribution of 25–75 μm. The glass abundance retrieved from the MSL of the sample XS-JFM-012 is 0 wt.%, and that of the sample XS-JFM-006 is negligible (0 wt.% orange glass and 1.3 wt.% green glass). The retrieved glass abundance of sample XS-JFM-015 is ~2 wt.%, and that of sample XS-JFM-009 is ~5 wt.%. As shown in Figure 6, the best-matched spectra of samples XS-JFM-009 and XS-JFM-015 from MSL with orange/green glass are quite different from the real mineral spectra. These unmatched spectra might result in the false detection of glass abundance.

We also compared the relative abundances of the other four minerals (OLV, OPX, CPX, and PLG) retrieved by the RLM, and the results are shown in Figure 6. The mineral abundance errors between the inversion and the real value of the XS-JFM-006 and XS-JFM-012 samples are less than 10 wt.%, while the other two samples have larger errors because of the unsatisfactory fitted spectra (Figure 6c,d,g,h). Using these mixed mineral samples, we found that inversion using the MSL in this work can prevent false detection of glass.

The above results indicate that the relative abundance difference between the MSL retrieval with glass considered and the real values can be significantly reduced, and the glass abundance can be retrieved qualitatively.

Table 3. The abundance of glasses obtained from the LSCC measurement and the MSL retrieval results.

Value (wt.%)	Soil ID (Highland)	X14141-5.7	X14163-57	X14259-85	X14260-72	X61141-56	X61221-9.2	X62231-91	X64801-82	X67461-25	X67481-31
Meas.	Agglutinates *	48.6	58.5	68.7	65.2	53.9	32.6	55.0	61.0	32.4	28.6
MSL	Orange glass	5.0	6.3	2.5	3.8	8.8	10.0	3.8	3.8	2.5	2.5
	Green glass	1.3	5.0	2.5	2.5	5.0	5.0	2.5	2.5	3.8	1.3
Value (wt.%)	Soil ID (Mare)	X12001-56	X12030-14	X15041-94	X15071-52	X70181-47	X71061-41	X71501-35	X79221-81	X10084-78	
Meas.	Agglutinates *	56.8	49.8	56.7	49.2	51.7	37.9	44.8	54.3	57.0	
	Volcanic glass	1.3	1.5	2.6	4.1	9.2	18.8	7.5	9.2	2.9	
MSL	Orange glass	6.3	12.5	7.5	2.5	6.8	18.8	13.8	12.5	17.5	
	Green glass	2.5	11.3	5.0	6.3	5.0	8.8	8.8	5.0	11.3	

* This designation effectively includes all impact-produced glasses, the majority (>90%) of which is agglutinitic glass; these are combined because they have similar compositions and both contain nanophase Fe. Meas. means measurement.

Table 4. The true and retrieved mineral abundances of four RELAB mixture samples. The samples of the RELAB contain five pure minerals with the sum of 100% (OLV+ OPX+ CPX+ PLG+ ILM = 100 wt.%). The abundances of the four main minerals and glasses (orange or green) (with OLV+ OPX+ CPX+ PLG+ glass = 100 wt.%) are retrieved by using the MSL. ILM is not included due to its lack of spectral features.

Sample ID	RELAB Data		Retrieved Abundance by MSL with Glass		
	Endmember of the Samples	Real Abundance (wt.%)	Endmember of the MSL	MSL Result (with Orange Glass) (wt.%)	MSL Result (with Green Glass) (wt.%)
XS-JFM-006	OLV	21	OLV	9.2	12.3
	OPX	11	OPX	3.5	6
	CPX	42	CPX	48.2	49.4
	PLG	23	PLG	39.1	31
	ILM	3	glass	0	1.3

Table 4. *Cont.*

Sample ID	RELAB Data		Retrieved Abundance by MSL with Glass		
	Endmember of the Samples	**Real Abundance (wt.%)**	**Endmember of the MSL**	**MSL Result (with Orange Glass) (wt.%)**	**MSL Result (with Green Glass) (wt.%)**
XS-JFM-009	OLV	30	OLV	2.9	8
	OPX	49	OPX	47.9	32.9
	CPX	10	CPX	10.1	25.5
	PLG	4	PLG	35.3	27.4
	ILM	7	glass	3.8	6.3
XS-JFM-012	OLV	5	OLV	2	3.1
	OPX	5	OPX	0	0
	CPX	47	CPX	66.5	65.9
	PLG	15	PLG	30.5	31
	ILM	28	glass	0	0
XS-JFM-015	OLV	23	OLV	11.2	13.3
	OPX	0	OPX	0	0
	CPX	0	CPX	16.1	20.1
	PLG	69	PLG	70.2	64.5
	ILM	8	glass	2.5	1.3

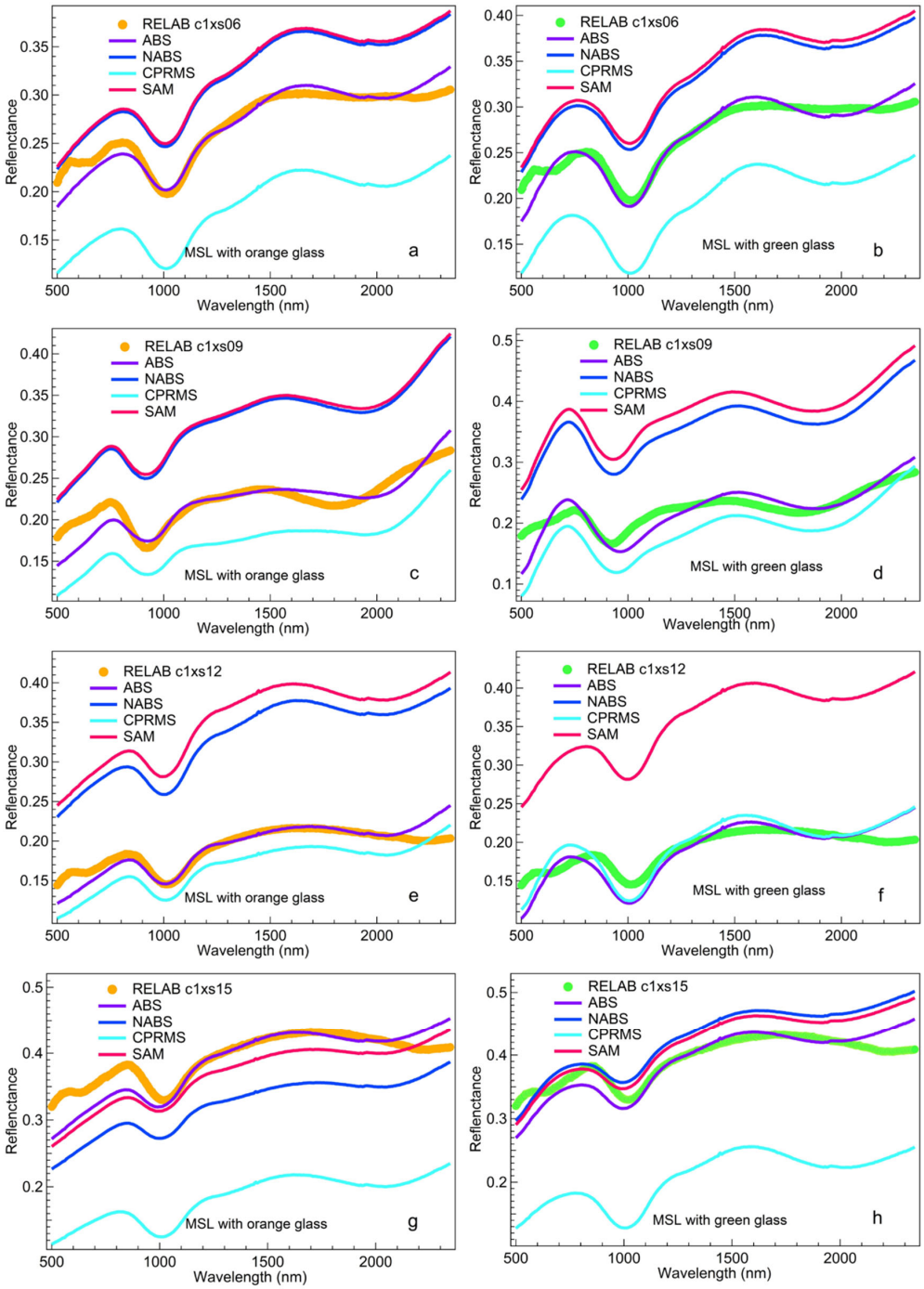

Figure 6. Comparisons of RELAB sample spectra with the corresponding best-matched MSL spectra (green or orange glass) were obtained using four different fitting metrics (Equations (15)–(18)). The results shown in (**a**,**c**,**e**,**g**) and those in (**b**,**d**,**f**,**h**) are obtained using the MSL with orange and green glasses, respectively. c1xs06, c1xs09, c1xs12, and c1xs15 are spectra ID corresponding to RELAB sample ID XS-JFM-006, XS-JFM-009, XS-JFM-012, and XS-JFM-006, respectively.

4. Applications to CE-3 In Situ Lunar Measurements

The CE-3 mission measured the lunar surface reflectance at Mare Imbrium and collected four spectra at different sites. Now we apply the MSL with glass to retrieve the abundances of major minerals and glass from CE-3 spectra in this section. The best-fitting results for the four measurements are shown in Figure 7, and the abundances of minerals and glass obtained by averaging the four metrics results are summarized in Table 5. The

abundances of glass retrieved from the MSL (~8.9 wt.% orange glass, ~5.7 wt.% green glass) are very close to the LSCC mare sample (~10.8 wt.% orange glass, ~7.1 wt.% green glass). Since the CE-3 landing site in Mare Imbrium is a typical lunar mare region, it is reasonable to expect its glass abundance to be similar to the LSCC mare samples.

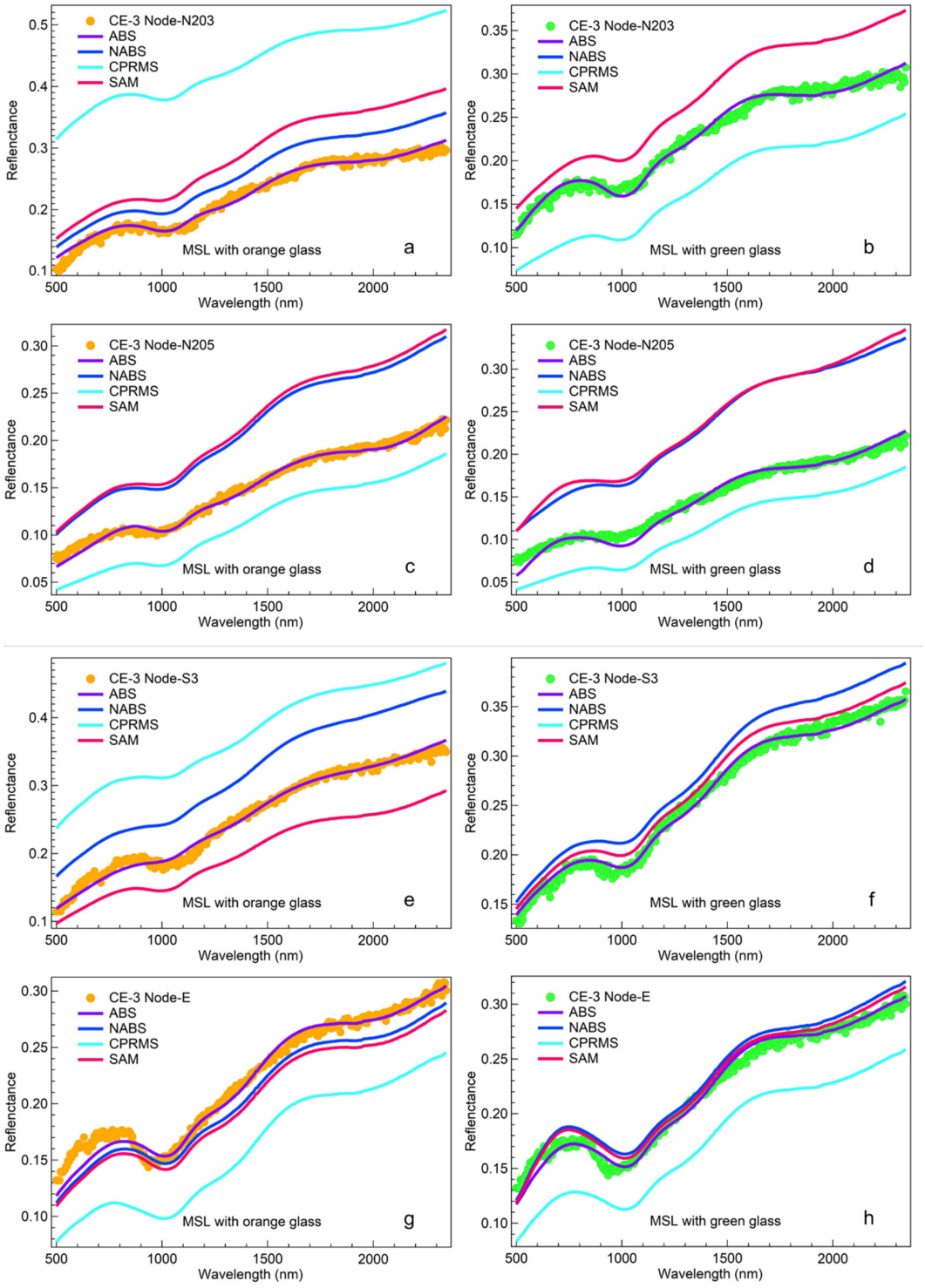

Figure 7. Comparisons of the CE-3 sample spectra with the corresponding best-matched MSL spectra (green or orange glass) were obtained using four different fitting metrics (Equations (15)–(18)). The results shown in (**a**,**c**,**e**,**g**) and those in (**b**,**d**,**f**,**h**) are obtained using the MSL with orange and green glasses, respectively.

Table 5. Mineral abundances (wt.%) were retrieved by comparing CE-3 data and the MSL with green/orange glass.

	MSL with Orange Glass (wt.%)					MSL with Green Glass (wt.%)					MSL without Glass (wt.%)			
Data	**OLV**	**OPX**	**CPX**	**PLG**	**glass**	**OLV**	**OPX**	**CPX**	**PLG**	**glass**	**OLV**	**OPX**	**CPX**	**PLG**
Node N203	17.8	3.5	27.8	46.0	5.0	16.8	0.0	36.0	43.3	3.8	23.8	6.0	46.9	23.3
Node N205	25.1	4.3	32.6	28.1	10.0	21.3	1.0	41.7	30.9	5.0	28.9	5.8	43.8	21.5
Node E	29.9	2.1	27.8	33.6	6.6	26.2	0.0	28.6	36.4	8.8	30.5	0.0	28.6	40.9
Node S3	19.7	1.8	25.5	39.3	13.8	20.2	3.1	32.2	39.5	5.0	23.1	13.1	44.6	19.2
(N205 + S3)/2	22.4	3.1	29.1	33.7	11.9	20.8	2.1	37.0	35.2	5.1	26.0	9.5	44.2	20.3
Average	23.1	2.9	28.4	36.8	8.9	21.4	1.0	34.4	37.5	5.7	26.5	6.2	41.0	26.2

The retrieved abundances of the four minerals using the MSL (Table 5) can be compared with the onboard Active Particle X-ray Spectrometer (APXS) measurements at Nodes S3 and N205. The APXS measurements indicate that the regolith at these two locations contains ~22 wt.% FeO, ~4 wt.% TiO_2, ~10 wt.% MgO, and ~0.14 wt.% K_2O, corresponding to mineral abundances of ~ 19 wt.% OLV, ~40 wt.% PXY, ~30 wt.% PLG, and ~7 wt.% ILM, based on normative mineralogy calculations [24]. We averaged the values retrieved by the MSL without glass (LUT) for Nodes S3 and N205 and found the OLV and PYX abundances retrieved from the LUT (~ 26 wt.% OLV, ~54 wt.% PXY) are higher than the measured value of APXS, and the PLG abundance (~30 wt.% PLG) is lower than the measured value. The mineral abundances obtained by the MSL with glass are closer to the APXS result.

5. Conclusions

We have constructed the spectral library of mixtures (MSL) of major lunar-type minerals and synthetic glasses by using a radiative transfer model. We found that, by adding glass as the endmember, the mineral abundance can be retrieved more accurately, and the glass abundance can be retrieved qualitatively. By applying the MSL with glass retrieval method to the in situ lunar data measured by the Chang'E-3 mission, we obtained mineral abundances close to the Active Particle X-ray Spectrometer measurement. In this work, only one of the synthetic volcanic glasses (green or orange) was added as an endmember of the MSL. In reality, however, the compositions and morphologies of lunar glasses are very diverse, and future efforts in considering more types of glasses in the spectral library would be expected. Also, we only concentrated on the 1000 nm absorption features of the lunar-type minerals and synthesis glasses in constructing the spectral library of the mixtures. For lunar impact glasses and minerals, including plagioclase and titanium oxide, that lack prominent absorption features in the visible and near-infrared region, their spectral features in the longer wavelength region, including the short-wavelength infrared (SWIR) and mid-infrared (MIR) may be used in spectral unmixing efforts. For example, it has been found [39] that lunar pyroclastic glasses, mare impact glasses, and highland impact glasses that lack VNIR spectra features exhibit different spectral features in the MIR region. Lunar soils also have rich spectral features in SWIR and MIR regions (e.g., [40]). Future efforts on spectral unmixing of lunar materials containing all types of glasses in SWIR and MIR, including measurements in simulated lunar environments, are expected to improve our capabilities in identifying the endmembers of mixtures using remote sensing spectral data.

Author Contributions: Conceptualization, X.H. and H.Z.; methodology, P.L. and H.Z.; software, X.H., T.J. and P.M.; validation, T.J. and P.M.; investigation, H.Z. and M.Z.; resources, H.Z.; data curation, X.H.; writing—original draft preparation, X.H.; writing—review and editing, P.M., T.J. and H.Z.; supervision, H.Z.; project administration, H.Z.; funding acquisition, H.Z. All authors have read and agreed to the published version of the manuscript.

Funding: This research was funded by the Natural Science Foundation of China (12073024) and the Civil Aerospace Pre-research Project (D020302).

Data Availability Statement: Data are available upon request.

Acknowledgments: The Chang'E-3 data can be downloaded from https://moon.bao.ac.cn/ceweb/ (accessed on 17 April 2023).

Conflicts of Interest: The authors declare no conflict of interest.

References

1. Lucey, P.G. Radiative transfer modeling of the effect of mineralogy on some empirical methods for estimating iron concentration from multispectral imaging of the moon. *J. Geophys. Res. Planets* **2006**, *111*, E08003. [CrossRef]
2. Shkuratov, Y.; Kaydash, V.; Korokhin, V.; Velikodsky, Y.; Opanasenko, N.; Videen, G. Optical measurements of the Moon as a tool to study its surface. *Planet. Space Sci.* **2011**, *59*, 1326–1371. [CrossRef]
3. Adams, J.B.; McCord, T.B. Optical properties of mineral separates, glass, and anorthositic fragments from Apollo mare samples. In *Lunar and Planetary Science Conference Proceedings*; Pergamon Press: New York, NY, USA, 1971; Volume 2, p. 2183.
4. Farr, T.G.; Bates, B.A.; Ralph, R.L.; Adams, J.B. Effects of overlapping optical absorption bands of pyroxene and glass on the reflectance spectra of lunar soils. In *Lunar and Planetary Science Conference Proceedings*; Pergamon Press: New York, NY, USA, 1980; Volume 11, pp. 719–729.
5. Pieters, C.M.; Noble, S.K. Space weathering on airless bodies. *J. Geophys. Res. Planets* **2016**, *121*, 1865–1884. [CrossRef]
6. Clénet, H.; Pinet, P.; Daydou, Y.; Heuripeau, F.; Rosemberg, C.; Baratoux, D.; Chevrel, S. A new systematic approach using the modified gaussian model: Insight for the characterization of chemical composition of olivines, pyroxenes and olivine–pyroxene mixtures. *Icarus* **2011**, *213*, 404–422. [CrossRef]
7. Klima, R.L.; Dyar, M.D.; Pieters, C.M. Near-infrared spectra of clinopyroxenes: Effects of calcium content and crystal structure. *Meteorit. Planet. Sci.* **2011**, *46*, 379–395. [CrossRef]
8. Pieters, C.M. Strength of mineral absorption features in the transmitted component of near-infrared reflected light: First results from RELAB. *J. Geophys. Res. Solid Earth* **1983**, *88*, 9534–9544. [CrossRef]
9. Besse, S.; Sunshine, J.M.; Gaddis, L.R. Volcanic glass signatures inspectroscopic survey of newly proposedlunar pyroclastic deposits. *J. Geophys. Res. Planets* **2014**, *119*, 355–372. [CrossRef]
10. Taylor, K.E. Summarizing multiple aspects of model performance in a single diagram. *J. Geophys. Res.* **2001**, *106*, 7183–7192. [CrossRef]
11. McKay, D.S.; Heiken, G.H.; Taylor, R.M.; Clanton, U.S.; Morrison, D.A.; Ladle, G.H. Apollo 14 soils: Size distribution and particle types. In *Lunar and Planetary Science Conference Proceedings*; Pergamon Press: New York, NY, USA, 1972; Volume 3, p. 983.
12. McKay, D.S.; Basu, A. The production curve for agglutinates in planetary regoliths. *J. Geophys. Res. Solid Earth* **1983**, *88*, B193–B199. [CrossRef]
13. Pieters, C.M.; Fischer, E.M.; Rode, O.; Basu, A. Optical effects of space weathering: The role of the finest fraction. *J. Geophys. Res. Planets* **1993**, *98*, 20817–20824. [CrossRef]
14. Wetzel, D.; Hauri, E.; Saal, A.; Rutherford, M. Carbon content and degassing history of the lunar volcanic glasses. *Nat. Geosci.* **2015**, *8*, 755–758. [CrossRef]
15. Scudder, N.A.; Horgan, B.H.; Rampe, E.B.; Smith, R.J.; Rutledge, A.M. The effects of magmatic evolution, crystallinity, and microtexture on the visible/near-infrared and thermal-infrared spectra of volcanic rocks. *Icarus* **2021**, *359*, 114344. [CrossRef]
16. Wilson, L.; Head, J.W., III. Ascent and eruption of basaltic magma on the Earth and Moon. *J. Geophys. Res. Solid Earth* **1981**, *86*, 2971–3001. [CrossRef]
17. Saal, A.E.; Hauri, E.H.; Cascio, M.L.; van Orman, J.A.; Rutherford, M.C.; Cooper, R.F. Volatile content of lunar volcanic glasses and the presence of water in the Moon's interior. *Nature* **2008**, *454*, 192–195. [CrossRef]
18. Arndt, J.; Engelhardt, W.V.; Gonzalez-Cabeza, I.; Meier, B. Formation of apollo 15 green glass beads. *J. Geophys. Res. Solid Earth* **1984**, *89*, C225–C232. [CrossRef]
19. Cannon, K.M.; Mustard, J.F.; Parman, S.W.; Sklute, E.C.; Dyar, M.D.; Cooper, R.F. Spectral properties of Martian and other planetary glasses and their detection in remotely sensed data. *J. Geophys. Res. Planets* **2017**, *122*, 249–268. [CrossRef]
20. Hapke, B. Bidirectional reflectance spectroscopy: 1. theory. *J. Geophys. Res. Planets* **1981**, *86*, 3039–3054. [CrossRef]
21. Lemelin, M.; Lucey, P.G.; Song, E.; Taylor, G.J. Lunar central peak mineralogy and iron content using the kaguya multiband imager: Reassessment of the compositional structure of the lunar crust. *J. Geophys. Res. Planets* **2015**, *120*, 869–887. [CrossRef]
22. Sun, L.; Lucey, P.G. Unmixing Mineral Abundance and Mg# With Radiative Transfer Theory: Modeling and Applications. *J. Geophys. Res. Planets* **2021**, *126*, e2020JE006691.
23. Cannon, K.; Mustard, J. Preserved glass-rich impactites on Mars. *Geology* **2015**, *43*, 635–638. [CrossRef]
24. Pieters, C.M.; Hanna, K.D.; Cheek, L.; Dhingra, D.; Prissel, T.; Jackson, C.; Taylor, L.A. The distribution of mg-spinel across the moon and constraints on crustal origin. *Am. Miner.* **2014**, *99*, 1893–1910. [CrossRef]
25. Denevi, B.W.; Yasanayake, C.N.; Jolliff, B.L.; Lawrence, S.J.; Hiroi, T.; Martin, A.C. The Spectral Properties of Lunar Agglutinates. In *Lunar and Planetary Science Conference*; Pergamon Press: New York, NY, USA, 2021; Volume 2548, p. 2368.

26. Zhang, H.; Yang, Y.; Yuan, Y.; Jin, W.; Lucey, P.G.; Zhu, M.-H.; Kaydash, V.G.; Shkuratov, Y.G.; Di, K.; Wan, W.; et al. In situ optical measurements of Chang'E-3 landing site in Mare Imbrium: 1. Mineral abundances inferred from spectral reflectance. *Geophys. Res. Lett.* **2015**, *42*, 6945–6950. [CrossRef]
27. Hu, X.; Ma, P.; Yang, Y.; Zhu, M.H.; Jiang, T.; Lucey, P.G.; Sun, L.; Zhang, H.; Li, C.; Xu, R.; et al. Mineral abundances inferred from in situ reflectance measurements of Chang'E-4 landing site in South Pole-Aitken basin. *Geophys. Res. Lett.* **2019**, *46*, 9439–9447. [CrossRef]
28. Morris, R.V. The surface exposure (maturity) of lunar soils: Some concepts and Is/FeO complication. In *Lunar and Planetary Science Conference Proceedings*; Pergamon Press: New York, NY, USA, 1978; Volume 9, pp. 2287–2297.
29. Taylor, L.; Cahill, J.; Patchen, A.; Pieters, C.; Morris, R.; Keller, L.; McKay, D. Mineralogical and chemical characterization of lunar highland regolith: Lessons learned from mare soils. In *Lunar and Planetary Science Conference*; Pergamon Press: New York, NY, USA, 2001; Volume 32, p. 2196.
30. Wang, Z.; Wu, Y.; Blewett, D.T.; Cloutis, E.A.; Zheng, Y.; Chen, J. Submicroscopic metallic iron in lunar soils estimated from the in situ spectra of the Chang'E-3 mission. *Geophys. Res. Lett.* **2017**, *44*, 3485–3492. [CrossRef]
31. Ling, Z.; Jolliff, B.L.; Wang, A.; Li, C.; Liu, J.; Zhang, J.; Li, B.; Sun, L.; Chen, J.; Xiao, L.; et al. Correlated compositional and mineralogical investigations at the Chang'e-3 landing site. *Nat. Commun.* **2015**, *6*, 8880. [CrossRef]
32. Hapke, B. *Theory of Reflectance and Emittance Spectroscopy*; Cambridge University Press: Cambridge, UK, 2012.
33. Mustard, J.F.; Pieters, C.M. Photometric phase functions of common geologic minerals and applications to quantitative analysis of mineral mixture reflectance spectra. *J. Geophys. Res. Planets* **1989**, *94*, 13619–13634. [CrossRef]
34. Lucey, P.G. Mineral maps of the moon. *Geophys. Res. Lett.* **2004**, *31*, L08701. [CrossRef]
35. Lucey, P.G.; Blewett, D.T.; Jolliff, B.L. Lunar iron and titanium abundance algorithms based on final processing of Clementine ultraviolet-visible images. *J. Geophys. Res. Planets* **2000**, *105*, 20297–20305. [CrossRef]
36. Hapke, B. Space weathering from mercury to the asteroid belt. *J. Geophys. Res. Planets* **2001**, *106*, 10039–10073. [CrossRef]
37. Taylor, L.; Patchen, A.; Taylor, D.; Chambers, J.; McKay, D. X-ray digital imaging and petrography of lunar mare soils: Data input for remote sensing calibrations. *Icarus* **1996**, *124*, 500–512. [CrossRef]
38. Sunshine, J.M.; Pieters, C.M. Estimating modal abundances from the spectra of natural and laboratory pyroxene mixtures using the modified Gaussian model. *J. Geophys. Res. Planets* **1993**, *98*, 9075–9087. [CrossRef]
39. Zeng, X.; Li, X.; Martin, D.; Tang, H.; Yu, W.; Liu, J.; Wang, S. Micro-FTIR spectroscopy of lunar pyroclastic and impact glasses as a new diagnostic tool to discern them. *J. Geophys. Res. Planets* **2019**, *124*, 3267–3282. [CrossRef]
40. Salisbury, J.W.; Basu, A.; Fischer, E.M. Thermal infrared spectra of lunar soils. *Icarus* **1997**, *130*, 125–139. [CrossRef]